Sensors and Actuators B 259 (2018) 97–105

Contents lists available at ScienceDirect

Sensors and Actuators B: Chemical

journal homepage: www.elsevier.com/locate/snb

Hydrodynamic rotating motion of micromotors from femtosecond laser microfabrication

Wei Guan[a,1], Chao Lv[a,1], Yi-Shi Xu[a], Yan-Hao Yu[a], Hong Xia[a,*], Li-Gang Niu[a], Sen Liu[a], Gong Wang[a], Ying-Shuai Wang[a], Hong-Bo Sun[a,b,*]

[a] State Key Laboratory of Integrated Optoelectronics, College of Electronic Science and Engineering, Jilin University, 2699 Qianjin Street, Changchun 130012, China

[b] State Key Lab of Precision Measurement and Instruments, Department of Precision Instrument, Tsinghua University, Haidian, Beijing 100084, China

ARTICLE INFO

Article history:
Received 24 July 2017
Received in revised form
23 November 2017
Accepted 26 November 2017
Available online 2 December 2017

Keywords:
Hydrodynamic motion
Micromotor
Rotating
Femtosecond laser microfabrication

ABSTRACT

The micro-motion of the machine is essential and valuable in environment, biology and medicine research. Environment-propelled micromotion can exhibit driven non-equilibrium behaviors. The energy conversation of micromotors from fluid environment would be an important power supply method for the distributed sensor network. Here, we report a kind of rotating motion of microturbines as micromotors driven by hydrodynamic liquid flow. By using femtosecond laser direct writing technology, the microturbine was fabricated, containing a simple and controllable structure of a fixed central axis and movable blades. The rotation speed could be controlled by the speed of flow, the blade tilt angle, the blade length and the blade number, and the rotation direction of microturbine could be decided by the tilt direction of blades. A dual linkage system constituted two microturbines could be designed and achieved. The ability to harness and control the power of motions appears an important requirement for further development of hydrodynamic flow-driven mechanical systems.

1. Introduction

In living systems of nature the motion is an essential process, which is indispensable for the achievement of mechanical functions in artificial systems, such as robots and machines. For artificial target objects, the physical, chemical or biospheric energy has been used to obtain motion of these objects [1–4]. The motion of micronano-objects containing special responsive component could be induced by light field, magnetic field, electric field, chemical gradient or non-equilibrium condition, and the motion could cease when the gradient disappears or an equilibrium condition is established [5–16]. Light momentum transfer of laser as mobile elements has been applied to trap and manipulate μm-sized solid particles [5–8]. The micro-structures remotely controlled by magnetic force have been created for swimming, mixing, and sensing by using various fabrication technology [10–12]. In addition, self-propelled catalytic micromotors and microgears driven by bacteria or Janus particles were reported [13–15,17–19].

In macro field, hydrodynamic power generation is an important power source form. The basic principle of the power generation is existence of water level difference, which can be transferred to the mechanical energy of the turbine. The mechanical energy drives the generator and gets the power. In micro-nano field hydrodynamic is also an important driving source [20]. For example, Hakansson et al. used hydrodynamic alignment with a dispersion-gel transition and prepared homogeneous and smooth filaments [21]. Kim et al. reported that the hydrodynamic shear flow aligned the microtubules translocating on a kinesin-coated surface in the direction parallel to the fluid flow [22,23]. Through microturbines, the kinetic energy of fluid can be converted into rotating mechanical energy, and furthermore can be converted into electricity. The hydrodynamic is an optimal energy acquisition method of underwater distributed sensor. In order to realize the large energy conversion efficiency, the microturbine requires a fine and complex structure.

Femtosecond laser direct writing (FsLDW) technology have shown special capability for fabricating movable micro-devices due to its unique characteristics including programmable designability, 3D point-by-point processing capability and high spatial resolution [24–35]. Due to these fascinating properties, the fabricated actuators by FsLDW are ingenious. In this respect, Shear et al. creatively fabricated microscopic 3D hydrogel actuators composed

* Corresponding authors.
E-mail addresses: hxia@jlu.edu.cn (H. Xia), hbsun@tsinghua.edu (H.-B. Sun).
[1] These authors contributed equally to this work.

https://doi.org/10.1016/j.snb.2017.11.162
0925-4005/

of photocrosslinked proteins by multiphoton lithography and demonstrated their capabilities as chemically responsive micromechanical elements [36]. Protein-based hydrogels are excellently smart materials, they also reported photoillumination smart valves based on 3D-printed proteins for control of bacterial microenvironments [37]. Shape-shifting 3D protein hydrogel microstructures were fabricated by FsLDW, which had controllable cross-linking density through modulation of the laser writing z-layer distance induced a PH-responsive shape change [38,39]. In addition, dynamically tunable protein microlenses were built up by FsLDW that could swell and shrink reversibly in response to changes in the surrounding solution [40]. Besides protein hydrogels, other responsive materials were used to construct microactuators. For example, Zeng et al. fabricated a microscopic walker based on liquid crystalline elastomers by laser direct writing, which can powered by light to achieve different autonomous movements, including random or directional walking, rotation or jumping [41].

Turbine is a rotary-type power machine which converts the energy of fluid into mechanical power. In macro mechanical field turbine is one of the main components, especially for the aero engine, gas turbine and steam turbine. In micro field environmentally flow-driven motors are able to convert spontaneously flow energy into mechanical activity to induce controllable micromotion. The micromotors are excellent candidates for constructing machines, detectors, and novel robots. In our previous research, micronanomachines including microspring and microturbine were fabricated, and due to the introduction of magnetic components in these micronanomachines, they were remotely manipulated by magnetic force [42–44]. Herein, we demonstrate a hydrodynamic-driven microturbine as rotating micromachine model. In order to achieve controllable rotation speed, the arbitrarily programmable microturbines blade number, size and tilt angle of microturbines were fabricated by using FsLDW technology. The energy conversion from flow will promote research for micro-device motion. In this research the fabricated microturbines unlike static micronanostructures or micronanodevices by FsLDW are movable. And the fabricated microturbines are rotatable, and can act as energy conversation device to harness flow energy. This work is capable to broaden the potential application of micronano fabrication of FsLDW.

2. Experiments

2.1. Preparation of photoresists

The components of the photoresist including benzil (BZ), 2-benzyl-2-(dimethylamino)-1-(4- morpholinophenyl) butan-1-one (BAMPB), methyl acrylate (MA) and pentaerythritol triacrylate (PETA), were all purchased from Sigma-Aldrich Company and used without purification. The powder of BZ (1.66 wt%) used as photoinitiator and BAMPB (1.20 wt%) used as photosensitizer were mixed and dissolved in MA (37.14 wt%). Then the crosslinker PETA (60.00 wt%) was added into the above solution and the mixture solution was taken by ultrasound for 10 min to ensure all the chemicals were mixed uniformly. The mixture solution became pale green, transparent and viscous. The photoresist was obtained.

2.2. Fabrication of microturbines

The Ti-sapphire laser beam (Spectra Physics 3960-X1BB, 790-nm central wavelength, 120-fs pulse width, 80-MHz repetition rate from a mode-locked) was tightly focused into the photoresist using a high-numerical-aperture oil-immersion objective lens (Olympus, × 100, numerical aperture = 1.45). The average laser power density measured before the objective lens was 8–10 mW μm^{-2}, the 100 nm scanning step length and 800-μs exposure duration of each voxel were adopted. A two-galvano-mirror set and a piezo stage (Physik Instrumente P-622.ZCD) was used to control the horizontal movement of the laser beam and vertical movements of the sample. The photoresist was pinpointly written according to computer processing data that converted by designed programs (3Ds Max). For instance in Fig. 4a: 3D microturbines with the top cap diameter of 8 μm, the height of 15.5 μm, the central axletree diameter of 3 μm, the bushing inside diameter of 5.5 μm, the blades thickness of 2 μm, and the range of the blade length (*d'*) of 6–18 μm were fabricated. After polymerization, the sample was immersed in acetone, all the unpolymerized parts were washed away, free suspending bushing with three blades was obtained. Similarly, various complicated micro/nanostructures would be readily fabricated on the substrates by FsLDW.

2.3. Measurement of the microturbines motion

The optical microscopy images and videos were taken by a transmission optical microscope with a 40 × (numerical aperture = 0.65) objective, the frame rate was 20 frames per second. The fabricated microturbines were put into acetone to observe their motion. The volume of acetone was 18 ml and a culture plate with a diameter of 5.5 cm was used. The nitrogen flow was produced by a small portable nitrogen cylinder which was equipped with a gas flowmeter. And using this equipment the homogeneous continuous acetone flow could be obtained. The evaporation of acetone induced about 5% of acetone volume decreasing during a period of 20 s, hardly influencing the liquid flow speed, as well as the rotation speed. The flow speed of the acetone can be regulated by controlling the flow of nitrogen. A water solution of 0.2 ml contained polystyrene (PS) microspheres with a concentration of 5% was added into the acetone as suspending microobjects to evaluate the flow speed of liquid. The diameter of the PS microspheres was about 5 μm, and the concentration of PS microspheres in liquid was about 0.06%, so when the N_2 induced the liquid flow, the PS microspheres moved with a speed same as the flow speed of liquid.

3. Results and discussion

3.1. Observation of flow-induced rotation of microturbines

The scheme of the hydrodynamic micromotor motion was shown in Fig. 1a. As hydrodynamic motor model the simple microturbine structure with a central axletree attached to the base on the substrate and three blades attached at the rotating bushing outside the fixed axletree was fabricated. A pre-programmed computer design and FsLDW technology were used to fabricate the microturbines from acrylate-based photopolymerizable resin (Fig. 1b). After fabrication and development, the microturbines were immersed in acetone. The suspending bushing with three blades as the movable part was free, and limited between the cap of central axletree and the base (Fig. 1c–d). The liquid acetone environment of micromotors was helpful to decrease the frictional resistance between the rotating bushing and the base, ensuring the microturbines move softly. A uniform and stable nitrogen flow was implemented on the surface of acetone, which can induce a continuous acetone flow. The flow speed of the acetone was evaluated by the motion of the suspending microobjects in the liquid (Supporting Information, Fig. S1). In acetone solution, the average speed V_m of PS microspheres with the diameter of 5 μm was similar to the flow speed $V_f = s/t$, in which the distance s could be obtained by tracking the trajectories of micospheres. When the fluid passed through the microturbine, the impact from fluid to the microturbine blades produced a driving torque to the microturbine. So the microturbine overcame the

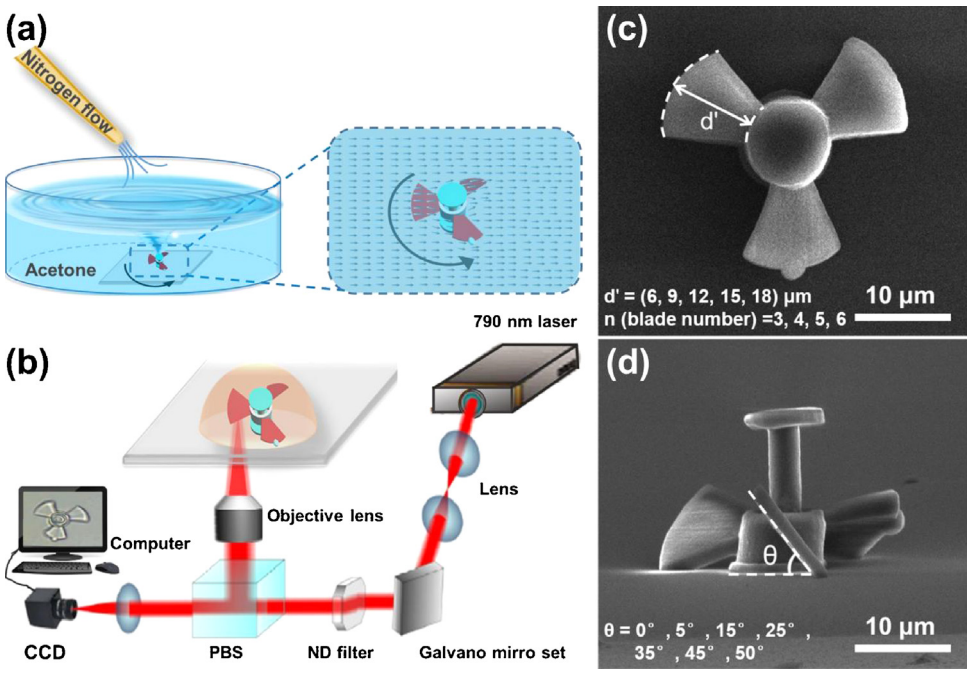

Fig 1. Experimental design. (a) Scheme of the experimental setup. (b) Schematic illustration for the FsLDW fabrication of microturbines. (c–d) The typical top-view and side-view SEM images of microturbine.

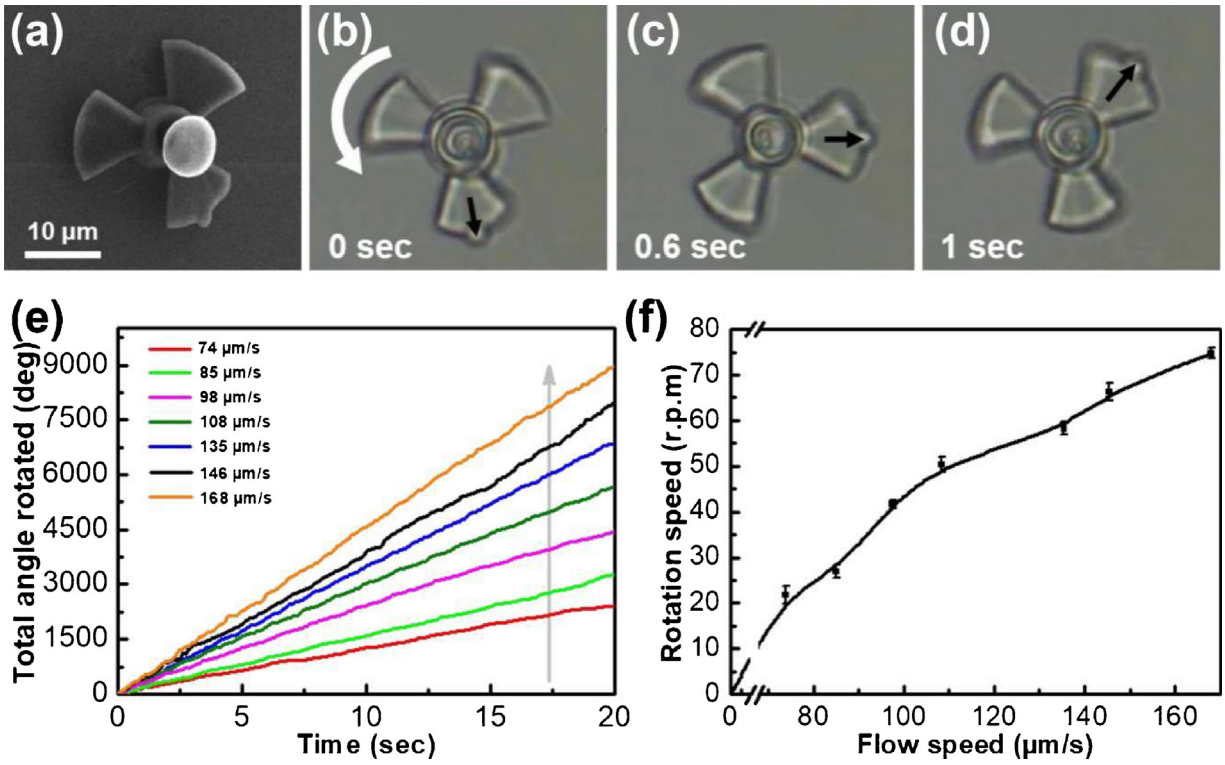

Fig. 2. Rotation of the microturbine in acetone. (a) SEM image of the rotation model microturbine. (b–d) Optical microscopy images of the rotation model microturbine in a circumgyratetion cycle. (e) Plot of the total angle rotated as a function of time for the microturbine under different flow speed levels. The arrow points towards the increasing of flow speed. (f) The average rotation speed as a function of flow speed for the microturbine.

friction torque and fluid resistance torque, and generated a rotation motion. When the flow speed was smaller than a minimum value, the microturbine was off and the thrust was nil. We selected a three-blade microturbine as rotation model, which had blade length of 9 μm, upper-left tilt angle of 35°, microturbine's height of approximately 15.5 μm, and the blade thickness of 2 μm (Fig. 2a). When the flow speed was 74 μm/s, a hydrodynamic pressure from the liquid flow induced the anticlockwise rotation of microturbine. The microturbine was observed by bright-field microscopy to record digital images at a frame rate of 20 fps. We filmed the rotary motor for 6 s (see Movie S1) and extracted angular velocity and rotation angle as the function of time by using a custom-made video

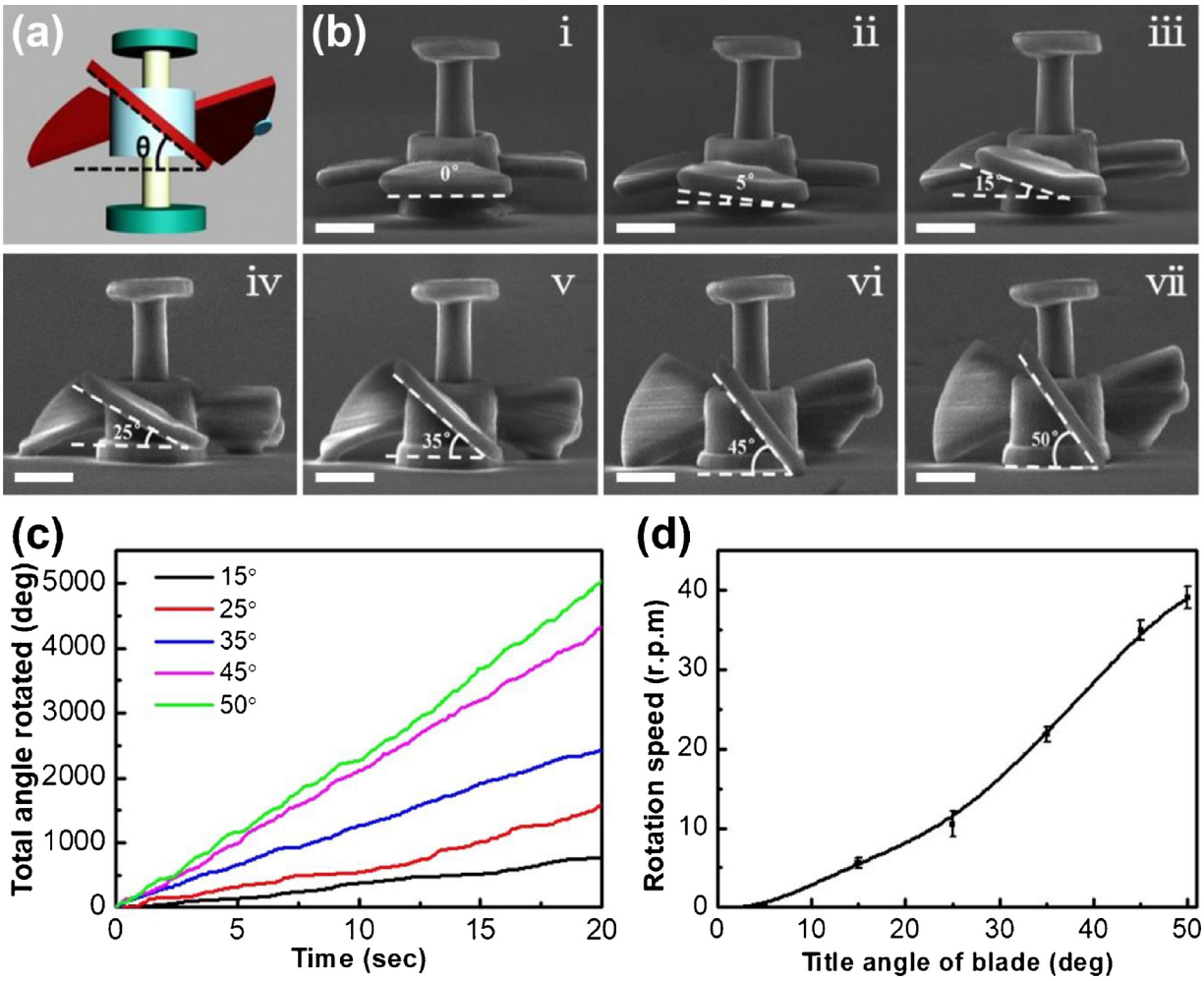

Fig. 3. Measurement of the rotational speed for microturbines with different blade tilt angles. (a) Front view schematic representation of the microturbines. (b) SEM images of the microturbines with different blade tilt angles. Scale bar: 5 μm. (c) Plot of total angle rotated as a function of time for the microturbine with different blade tilt angle. (d) The average rotation speed as a function of blade tilt angle for the microturbines. The liquid flow speed was 74 μm/s.

tracking routine (Fig. 2b–d). The average rotation frequency of 22 r.p.m was reached. Next, the torque of microturbine rotation was considered. Immersing inside liquid, the torque exerted on the turbine can be estimated as a balanced viscous torque $T \sim f_r \omega$, where ω is the angular velocity, and f_r is the rotational drag. The liquid flow with different flow speeds of 74–168 μm/s were performed, and the cumulative angles and rotation speeds of the microturbine at different flow speeds were calculated (Fig. 2e and f). The rotation rate increased with the increase in the speed of acetone flow as expected. Moreover, we observed that the blades of microturbines slightly shook during the rotation process due to space between the bushing and the central axis. The rotation shaken of microturbine was clear defined by the trajectories plot in Fig. S2 for 20 s under the flow speed of 74 μm/s.

3.2. The relationship between microturbine's rotation direction and blade orientation

In above-mentioned microturbine with upper-left tilt blade, the rotation direction was anticlockwise. To control the rotation direction, the microturbines with three different blade orientations, upper-left tilt, parallel to substrate and upper-right tilt, were fabricated. No rotation was observed for the turbine with blade parallel to substrate, only slightly shaking motion occurred. The acetone flow direction was roughly parallel to the blades, due to undersized stress area the total torque was too small to produce enough thrust. In many repetitive testing experiments, including changing the flow direction of liquid, the microturbines with upper-left tilt direction blades always rotated anticlockwise. Conversely, the microturbines with upper-right tilt direction blades always rotated clockwise (see Fig. S3 and Movie S2). In order to explain this phenomenon, we selected the microturbine with upper-left tilt direction blades as an example (Supporting Information, Fig. S4). Kept a constant flow direction (Fig. S4a), the acetone flow was divided into two parts roughly: active part (black arrows in Fig. S4b and c) and negative part (white arrows in Fig. S4b and c). When the fluid came, the active part of the acetone flow would change the flow direction according to the shape of blades due to the wall-attachment effect [45,46]. In other words, the tilting blades would bind the flow of fluid. θ side ($0^\circ < \theta \leq 50^\circ$) bound more fluid than α side ($130^\circ \leq \alpha < 180^\circ$), due to the gravity and viscous friction of the substrate. At the θ side the fluid kinetic energy was converted into mechanical energy more effectively, because more fluid was bounding. Microturbines' blades with the same bending direction led to the continuously anticlockwise rotation.

3.3. The relationship between rotation rate and blade parameters

With regard to rotating movement of microturbines under hydrodynamic stimulation, a stronger ability of mechanic output

is important. Because the blade in microturbine is the carrier of energy conversion, the blade parameters are primary factors to determine the performance of microturbine. Therefore we adjusted the blade parameters including the tilt angle, the blade length and the blade number. The microturbines with different tilt angle of blades of 0°, 5°, 15°, 25°, 35°, 45° and 50° were fabricated (Fig. 3a and b). The same liquid flow (speed of 74 μm/s) was performed to drive the microturbines, and microturbine motions were recorded in Movie S3. For the tilt angle of 0° and 5°, microturbines could not rotate. When the tilt angle of blade reached 15°, a rotating motion could be realized at an average rotation frequency of about 6 r.p.m (Fig. 3d). At larger tilt angle of 25°–50° the rotation speed of microturbines increased with increasing of the tilt angle. Time evolution of the cumulative rotation angle of the microturbines was shown in Fig. 3c. We selected microturbine with tilt angle of 35° ($\omega = 2\,rad\,s^{-1}, \sim 20$ *r.p.m*) as the rotation model to calculate the mechanical output power. The flow power is given by $P_f = 0.5\,mV_{\mu 1}{}^2$ according to classical mechanics, in which m is the flow mass per unit time. We can estimate the value of P_m in a rough way, when the acetone flow passed through the microturbines. The angular momentum changed only caused by M' (the torque of the micreturbines blades). We get $M' = \rho Q_e(V_{\mu 2} - V_{\mu 1})a$, where ρ is the density of acetone solution, Q_e is the effective flow, $V_{\mu 1}$ is the flow speed and $V_{\mu 2}$ (Supporting Information, Fig. S5) is the final flow speed after working [47]. Apparently $M = -M' = \rho Q_e(V_{\mu 1} - V_{\mu 2})a$, with M being the flow torque acted on the microturbines. The value of P_m can be obtained as the product of the torgue M and the rotation angular velocity ω. That is, $P_m = \rho Q_e(V_{\mu 1} - V_{\mu 2})a\omega$, which equals $\sim 1.2 \times 10^{-20}$ W. We can estimate the efficiency η of the flow-to-work conversion as the ratio between the flow power P_f and the mechanical power P_m, we get $\eta = P_m/P_f = 18\%$. Because of the energy loses that would occur when harvesting the energy during the motion of the microturbine the actual efficiency would be lower than this calculated value.

The dependence of microturbines rotation rate on the blade length was studied (Movie S4). Kept constant flow speed (74 μm/s) and the blade tilt angle (upper-left tilt angle of 35°), only the values of *d'* was adjusted (Fig. 4a and b). Fig. 4c showed the cumulative angle of the microturbines for different blade length under the same flow speed. We observed the increase of the rotation rate at the blade length larger than 6 μm. Moreover, at the blade length larger than 15 μm the rotation rate decreased (Fig. 4d).

Furthermore, to improve the microturbine performance, the effect of blade number on the motion of the microturbines was studied (Movie S5). Microturbines with four blades, five blades, and six blades were fabiricated with the same blade tilt angle and blade length (Fig. 5a). Fig. 5b showed the cumulative angle of the microturbines with three, four and five blades increased linearly with time, and the microturbine with five blades had the largest angular velocity. Theoretically, the more number of blades would cause larger flow stress area and larger torque, resulting in larger angular velocity. But the angular velocity from microturbine with six blades decreased with time, which is attributed to a heavier self-weight and a greater inertia for the microturbine with six blades. The driving of microturbine with six blades was more difficult than five blades one. Moreover, we observed that after stopping the nitrogen flow the microturbines with 5 or 6 blades would keep rotating for several seconds due to the greater inertia. Conversely, when the nitrogen flow was turn off the microturbines rotating with 3 or 4 blades would immediately stop. Furthermore, to assess the stability of rotation motion of microturbines the curves of angle diff to time for the microturbines with different blade number were shown in Fig. 5c. The values of all angle differentiation for four microturbines were larger than zero, meaning that during rotation process the angle was increasing with time. All four curves showed a significant fluctuation of angle differentiation. For the four microturbines, the microturbine with three blades showed a similar periodic fluctuation with the average fluctuation frequency of about 0.2 s and the average fluctuation amplitude of approximately 210°/s, which was probably originated from the periodic vibration of three blades under hydrodynamic flow. The microturbines with four, five and six blades showed a random fluctuation of angle diff.

To sum up, we studied the dependence of the microturbine rotation rate on the blade parameters, including the tilt angle, the blade length as well as the blade number. The energy conversion efficiency is an important parameter, and we tried to obtain the largest energy conversion efficiency value. We controlled all the other parameters to remain the same, when we studied the effect of each parameter on the microturbines rotation rate. By many testing experiments, the microturbine with optimized structure (blade tilt angle of 50°, blade length of 15 μm, blade number of 5) enable the largest energy conversion efficiency.

Here the micromotor rotation could not directly generate electronic energy to be applied for power supply of devices. To further obtain electronic energy from the micromotor rotation, a model of converting flow energy to electricity can be designed. In the model a magnet with size of several micrometers is attached on the surface of the blade of microturbine by laser tweezers, and a coil is placed on the substrate. When flow drives the microturbine rotation, a change in the magnet flux of coil is induced, thus generating electromotive forces. According to the calculation of the references, we roughly estimate the voltage value is a few nano volts [48,49]. The nano volt generators mainly have potential application towards next generation nano-devices, which may require small voltage, probably the nano volt range. In the future arrays of microturbines and further advances to the system may increase the power output, and contributes to miniaturization and integration of micronano devices and systems.

3.4. Synchronous rotation of two microturbines

Due to the dependence of rotation direction of microturbine on the blade tilt angle, a dual linkage system could be designed and achieved. Fig. 6 and Movie S6 showed both-turbine systems in which two microturbines have the same height and blade length, but different blade tilt angle. Meanwhile the distance between the centers of two microturbines was less than the diameter of each microturbine. In Fig. 6a two microturbines in system had the opposite blade orientation. For the left microturbines and the right microturbines, the blade tilt angles were 35°, and the blade orientations were upper-right and upper-left, respectively. At acetone flow (74 μm/s) the synchronous rotation of the two interdigitated microturbines at the same rotation speed of 16 r.p.m was observed. Due to the design of blade tilt angle in the synchronous rotation system, the rotation of left microturbine was clockwise, and the rotation of right microturbine was anticlockwise. The symmetric rotation direction could ensure unhindered work of the synchronous system. In the both-turbine systems two microturbines were active under hydrodynamic stimulation. In addition, we studied synchronous system including active and passive rotation. Two microturbines with different blade orientations (upper-right tilt angle of 35° and parallel to substrate) were fabricated on a slide (Fig. 6b). After acetone flow (74 μm/s) was added to the sample, the microturbine with upper-right tilt direction had an actively clockwise rotation and drove the one with blades parallel to substrate one. The microturbine with blades parallel to substrate started approximately synchronous rotating but with opposite direction as passive rotation. From Movie S6, the active rotation of blades was staccato, which is attributed to the energy loss to drive the passive microturbine. Sometimes blades of the two microturbines were stagger, which reduced the rate

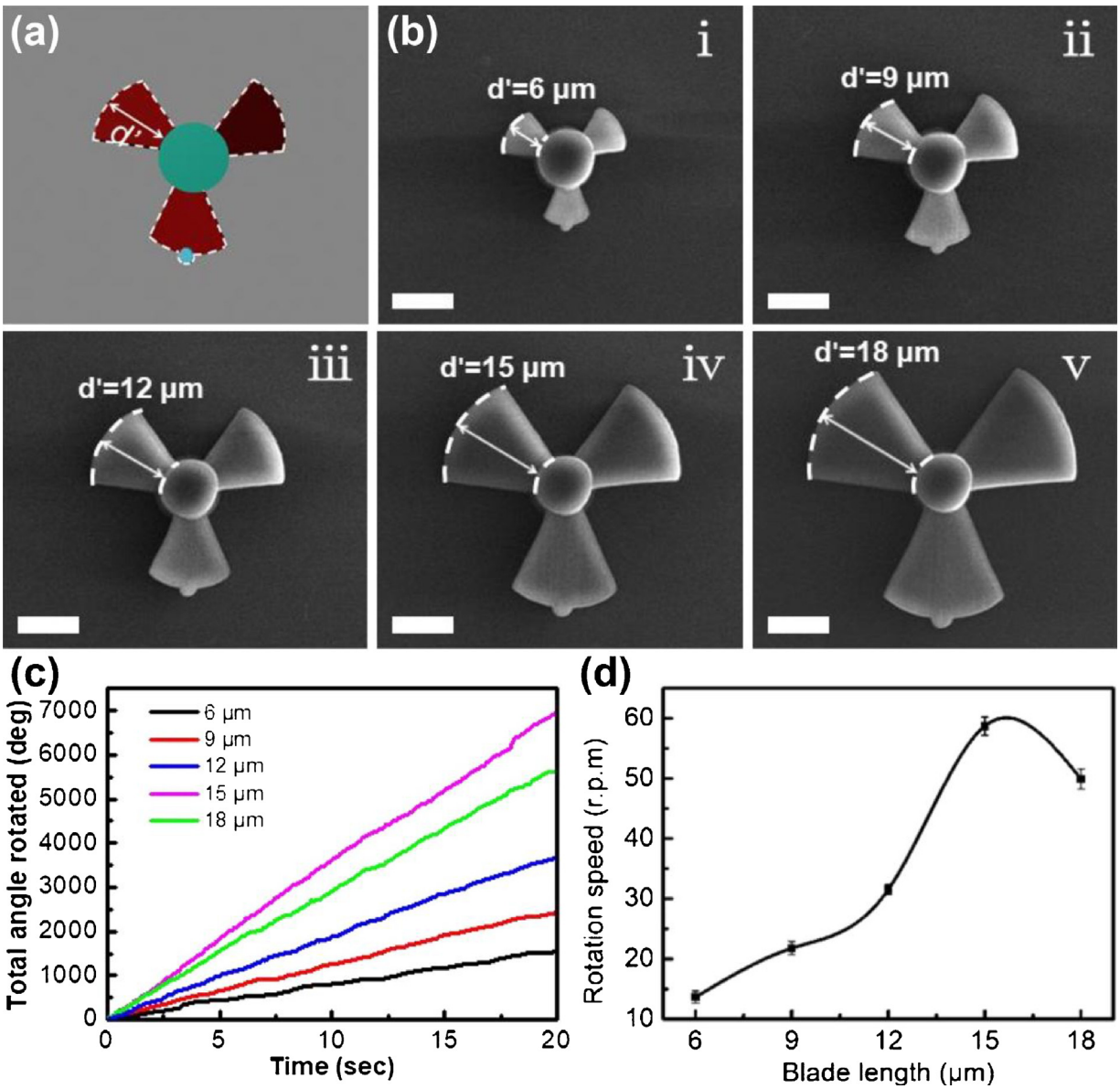

Fig. 4. Measurement of the rotational speed for microturbines with different blade lengths. (a) Planform schematic representation of the microturbines. (b) SEM images of the microturbines with different blade lengths. Scale bar: 10 μm. (c) Plot of total angle rotated as a function of time for the microturbines with different blade lengths. (d) The average rotation speed as a function of blade length for the microturbines. The liquid flow speed was 74 μm/s.

of synchronization. The blades of the two microturbines were not fully fitted, which was different from the gearing structure. Moreover, we fabricated two microturbines with the same blade orientation (upper-right tilt angle of 35°). As expected, no rotation was observed because of the strangled blades (shown in Movie S6).

The fabricated microturbines are developed by using acetone, and then driven to rotate in the acetone liquid environment. The liquid environment was changed to water or ethanol, no rotation motion of the microturbine would be observed. We supposed capillary sticking is the main reason to inhibit rotation when the developing liquid is exchanged. Water is pollution-free, green, and optimally fluid-driven liquid environment. Here this microturbine is a model system and would need to be modified to work in a relevant aqueous environment. If some water soluble photoresists, like bovine serum albumin, are used to fabricate microturbines, water can be used as developing liquid and working environment [35–40]. In addition, a grafting strategy has potential to establish hydrophilic coating to hydrophobic resin to work in an aqueous environment [50,51].

4. Conclusions

Because FsLDW technology has the abilities of readily adjustable computer-assistant 3D design and point by point fabrication, the variously parameters-adjusted microturbines were fabricated. The AFM image of the microturbine surface (Fig. S6) showed the low surface roughness, and decreasing of reducing friction. We demonstrated that the rotation rates could be continuously controlled by adjusting the speed of flow, the blade tilt angle, the blade length and the blade number. And the rotation direction only depended on the blade orientation. The dual linkage system could be designed and achieved. Applications at the micrometer scale, such microturbines as separators, sensors and mixers for microfluidics are the most promising. Moreover the sample fundamental motivation came from nitrogen flow which can be replaced by air flow i.e. the wind.

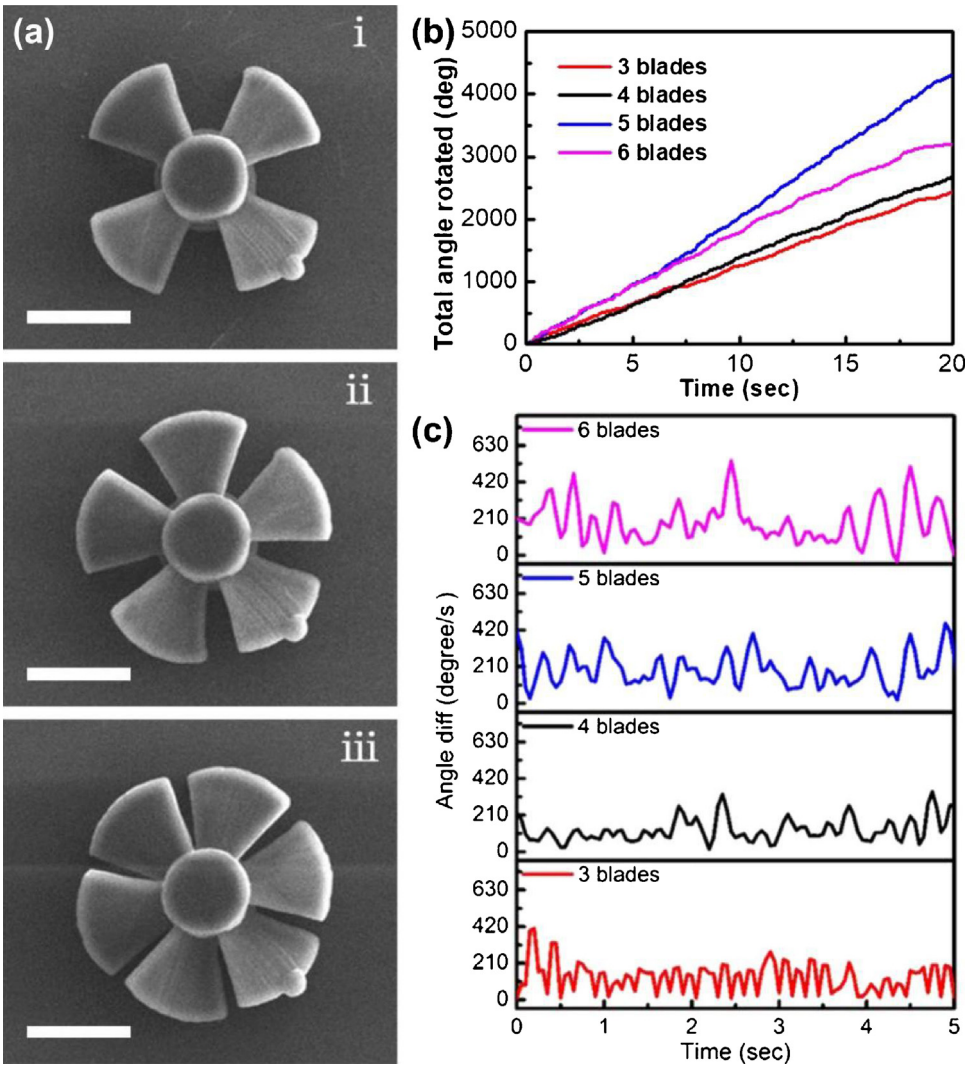

Fig. 5. Measurement of the rotational speed for microturbines with different blade number. (a) SEM images of the microturbines with different blade number. Scale bar: 10 μm. (b) Plot of total angle rotated as a function of time for the microturbines with different blade number. (c) Time fluctuations of angle diff for the microturbines with different blade number. The liquid flow speed was 74 μm/s.

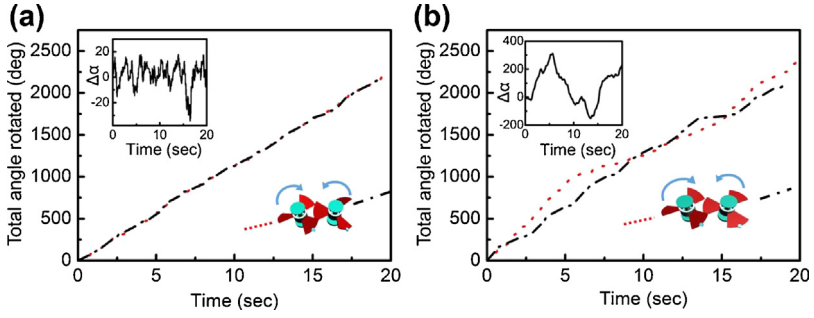

Fig. 6. Synchronous rotation. Total angle rotated as a function of time for a system of two microturbines. The inset plots the difference Δα in the rotation angles. (a) Red lines (dashed lines) refer to the microturbine with blade upper-right tilt angle of 35°. Black lines (dash-dotted lines) refer to the microturbine with blade upper-left tilt angle of 35°. The two microturbines have opposite blade tilt angle, resulting in opposite rotation directions. (b) Red lines (dashed lines) refer to the microturbine with blade upper-right tilt angle of 35°. Black lines (dash-dotted lines) refer to the microturbine with blades parallel to substrate. Under the acetone flow, the microturbine with upper-right tilt direction presented actively clockwise rotation and drove the parallel to substrate one to rotate in the opposite direction. The liquid flow speed was 74 μm/s. (For interpretation of the references to colour in this figure legend, the reader is referred to the web version of this article.)

The fabricated microturbines unlike static micronanostructures or micronanodevices by FsLDW were movable. And the fabricated microturbines were rotatable, and can act as energy conversation device to harness flow energy. This work is capable to broaden the potential application of micronano fabrication of FsLDW. In particular, such microstructures would have great potential in applications such as micro-generator driven by renewable energy in the field of micro-integrated circuit. We also believe that understanding and exploiting these complex hydrodynamic mechanisms may provide novel strategies to design autonomous micromachines.

Acknowledgments

This work was supported by the National Natural Science Foundation of China (Grant Nos. 61435005, 51335008, 51373064, 61378053, 61590930, and 91423102).

Appendix A. Supplementary data

Supplementary data associated with this article can be found, in the online version, at https://doi.org/10.1016/j.snb.2017.11.162.

References

[1] A. Sidorenko, T. Krupenkin, A. Taylor, P. Fratzl, J.R. Aizenberg, Reversible switching of hydrogel-actuated nanostructures into complex micropatterns, Science 315 (2007) 487–490.
[2] X.M. He, M. Aizenberg, O. Kuksenok, L.D. Zarzar, A. Shastri, A.C. Balazs, J. Aizenberg, Synthetic homeostatic materials with chemo-mechano-chemical self-regulation, Nature 487 (2012) 214–218.
[3] H.-B. Sun, K. Takada, S. Kawata, Elastic force analysis of functional polymer submicron oscillators, Appl. Phys. Lett. 79 (2001) 3173–3175.
[4] A. Sokolov, M.M. Apodaca, B.A. Grzybowski, I.S. Aranson, Swimming bacteria power microscopic gears, Proc. Natl. Acad. Sci. 107 (2010) 969–974.
[5] P. Galajda, P. Ormos, Rotors produced and driven in laser tweezers with reversed direction of rotation, Appl. Phys. Lett. 80 (2002) 4653.
[6] S. Maruo, H. Inoue, Optically driven viscous micropump using a rotating microdisk, Appl. Phys. Lett. 91 (2007) 084101.
[7] X.-F. Lin, G.-Q. Hu, Q.-D. Chen, L.-G. Niu, Q.-S. Li, A. Ostendorf, H.-B. Sun, A light-driven turbine-like micro-rotor and study on its light-to-mechanical power conversion efficiency, Appl. Phys. Lett. 101 (2012) 113901.
[8] D. Baigl, Photo-actuation of liquids for light-driven microfluidics: state of the art and perspectives, Lab Chip 12 (2012) 3637–3653.
[9] E. Uchida, R. Azumi, Y. Norikane, Light-induced crawling of crystals on a glass surface, Nat. Commun. 6 (2015) 7310.
[10] S. Tottori, L. Zhang, F.M. Qiu, K.K. Krawczyk, A. Franco-Obregon, B.J. Nelson, Magnetic helical micromachines: fabrication, controlled swimming, and cargo transport, Adv. Mater. 24 (2012) 811–816.
[11] S.Y. Lee, S. Yang, Fabrication and assembly of magneto-responsive anisotropic, and hybrid microparticles of variable size and shape, Angew. Chem. Int. Ed. 52 (2013) 8160–8164.
[12] A.G. Gillies, J. Kwak, R.S. Fearing, Controllable particle adhesion with a magnetically actuated synthetic gecko adhesive, Adv. Funct. Mater. 23 (2013) 3256–3261.
[13] Y.-S. Wang, H. Xia, C. Lv, L. Wang, W.-F. Dong, J. Feng, H.-B. Sun, Self-propelled micromotors based on Au–mesoporous silica nanorods, Nanoscale 7 (2015) 11951–11955.
[14] V.V. Singh, F. Soto, K. Kaufmann, J. Wang, Micromotor-based energy generation, Angew. Chem. Int. Ed. 54 (2015) 6896–6899.
[15] J. Zhang, Y.Y. Yao, L. Sheng, J. Liu, Self-fueled biomimetic liquid metal mollusk, Adv. Mater. 27 (2015) 2648–2655.
[16] M.M. Song, M.J. Cheng, M. Xiao, L.N. Zhang, G.N. Ju, F. Shi, Biomimicking of a swim bladder and its application as a mini-generator, Adv. Mater. 29 (2017) 1603312.
[17] C. Maggi, F. Saglimbeni, M. Dipalo, F. De Angelis, R. Di Leonardo, Micromotors with asymmetric shape that efficiently convert light into work by thermocapillary effects, Nat. Commun. 6 (2015) 7855.
[18] R. Di Leonardo, L. Angelani, D. Dell'Arciprete, G. Ruocco, V. Iebba, S. Schippa, M.P. Conte, F. Mecarini, F. De Angelis, E. Di Fabrizio, Bacterial ratchet motors, Proc. Natl. Acad. Sci. 107 (2010) 9541–9545.
[19] C. Maggi, J. Simmchen, F. Saglimbeni, J. Katuri, M. Dipalo, F. De Angelis, S. Sanchez, R. Di Leonardo, Self-assembly of micromachining systems powered by Janus micromotors, Small 12 (2016) 446–451.
[20] T. Franosch, M. Grimm, M. Belushkin, F.M. Mor, G. Foffi, L. Forro, S. Jeney, Resonances arising from hydrodynamic memory in Brownian motion, Nature 478 (2011) 85–88.
[21] K.M.O. Hakansson, A.B. Fall, F. Lundell, S. Yu, C. Krywka, S.V. Roth, G. Santoro, M. Kvick, L.P. Wittberg, L. Wagberg, L.D. Söderberg, Hydrodynamic alignment and assembly of nanofibrils resulting in strong cellulose filaments, Nat. Commun. 5 (2014) 4018.
[22] T. Kim, M.T. Kao, E. Meyhofer, E.F. Hasselbrink, Biomolecular motor-driven microtubule translocation in the presence of shear flow: analysis of redirection behaviours, Nanotechnology 18 (2007) 025101.
[23] T. Kim, E. Meyhofer, E.F. Hasselbrink, Biomolecular motor-driven microtubule translocation in the presence of shear flow: modeling microtubule deflection due to shear, Biomed. Microdevices 9 (2007) 501–511.
[24] B. Kaehr, D.A. Scrymgeour, Direct-write graded index materials realized in protein hydrogels, Appl. Phys. Lett. 109 (2016) 123701.
[25] D. Serien, S. Takeuchi, Fabrication of submicron proteinaceous structures by direct laser writing, Appl. Phys. Lett. 107 (2015) 013702.
[26] J.L. Connell, E.T. Ritschdorff, M. Whiteley, J.B. Shear, 3D printing of microscopic bacterial communities, Proc. Natl. Acad. Sci. 110 (2013) 18380–18385.
[27] Y.-L. Sun, W.-F. Dong, L.-G. Niu, T. Jiang, D.-X. Liu, L. Zhang, Y.-S. Wang, Q.-D. Chen, D.-P. Kim, H.-B. Sun, Protein-based soft micro-optics fabricated by femtosecond laser direct writing, Light: Sci. Appl. 3 (2014) e129.
[28] D. Wu, J. Xu, L.-G. Niu, S.-Z. Wu, K. Midorikawa, K. Sugioka, In-channel integration of designable microoptical devices using flat scaffold-supported femtosecond-laser microfabrication for coupling-free optofluidic cell counting, Light: Sci. Appl. 4 (2015) e228.
[29] C.Y. Khripin, C.J. Brinker, B. Kaehr, Mechanically tunable multiphoton fabricated protein hydrogels investigated using atomic force microscopy, Soft Matter 6 (2010) 2842–2848.
[30] M. Malinauskas, A. Zukauskas, G. Bickauskaite, R. Gadonas, S. Juodkazis, Mechanisms of three-dimensional structuring of photo-polymers by tightly focussed femtosecond laser pulses, Opt. Express 18 (2010) 10209–10221.
[31] M. Malinauskas, A. Žukauskas, S. Hasegawa, Y. Hayasaki, V. Mizeikis, R. Buividas, S. Juodkazis, Ultrafast laser processing of materials: from science to industry, Light: Sci. Appl. 5 (2016) e16133.
[32] Y.-L. Sun, Q. Li, S.-M. Sun, J.-C. Huang, B.-Y. Zheng, Q.-D. Chen, Z.-Z. Shao, H.-B. Sun, Aqueous multiphoton lithography with multifunctional silk-centred bio-resists, Nat. Commun. 6 (2015) 8612.
[33] L.D. Zarzar, P. Kim, M. Kolle, C.J. Brinker, J. Aizenberg, B. Kaehr, Direct writing and actuation of three-dimensionally patterned hydrogel pads on micropillar supports, Angew. Chem. Int. Ed. 50 (2011) 9356–9360.
[34] Y.L. Hu, Z.X. Lao, B.P. Cumming, D. Wu, J.W. Li, H.Y. Liang, J.R. Chu, W.H. Huang, M. Gu, Laser printing hierarchical structures with the aid of controlled capillary-driven self-assembly, Proc. Natl. Acad. Sci. 112 (2015) 6876–6881.
[35] E.C. Spivey, E.T. Ritschdorff, J.L. Connell, C.A. McLennon, C.E. Schmidt, J.B. Shear, Multiphoton lithography of unconstrained three-dimensional protein microstructures, Adv. Funct. Mater. 23 (2013) 333–339.
[36] B. Kaehr, J.B. Shear, Multiphoton fabrication of chemically responsive protein hydrogels for microactuation, Proc. Natl. Acad. Sci. 105 (2008) 8850–8854.
[37] J.L. Connell, E.T. Ritschdorff, J.B. Shear, Three-dimensional printing of photoresponsive biomaterials for control of bacterial microenvironments, Anal. Chem. 88 (2016) 12264–12271.
[38] C.L. Lay, M.R. Lee, H.K. Lee, I.Y. Phang, X.Y. Ling, Transformative two-dimensional array configurations by geometrical shape-shifting protein microstructures, ACS Nano 9 (2015) 9708–9717.
[39] M.R. Lee, I.Y. Phang, Y. Cui, Y.H. Lee, X.Y. Ling, Shape-shifting 3D protein microstructures with programmable directionality via quantitative nanoscale stiffness modulation, Small 11 (2015) 740–748.
[40] Y.-L. Sun, W.-F. Dong, R.-Z. Yang, X. Meng, L. Zhang, Q.-D. Chen, H.-B. Sun, Dynamically tunable protein microlenses, Angew. Chem. Int. Ed. 51 (2012) 1558–1562.
[41] H. Zeng, P. Wasylczyk, C. Parmeggiani, D. Martella, M. Burresi, D.S. Wiersma, Light-fueled microscopic walkers, Adv. Mater. 27 (2015) 3883–3887.
[42] H. Xia, J. Wang, Y. Tian, Q.-D. Chen, X.-B. Du, Y.-L. Zhang, Y. He, H.-B. Sun, Ferrofluids for fabrication of remotely controllable micro-nanomachines by two-photon polymerization, Adv. Mater. 22 (2010) 3204–3207.
[43] J. Wang, H. Xia, B.-B. Xu, L.-G. Niu, D. Wu, Q.-D. Chen, H.-B. Sun, Remote manipulation of micronanomachines containing magnetic nanoparticles, Opt. Lett. 34 (2009) 581–583.
[44] Y. Tian, Y.-L. Zhang, H. Xia, L. Guo, J.-F. Ku, Y. He, R. Zhang, B.-Z. Xu, Q.-D. Chen, H.-B. Sun, Solvent response of polymers for micromachine manipulation, Phys. Chem. Chem. Phys. 13 (2011) 4835–4838.
[45] M. Miozzi, F. Lalli, G.P. Romano, Experimental investigation of a free-surface turbulent jet with Coanda effect, Exp. Fluids 49 (2010) 341–353.
[46] S. Chelikani, E.M. Sparrow, Numerical simulations of plane-wall Coanda effects for control of fiber trajectories in the Melt-Blown process, Ind. Eng. Chem. Res. 52 (2013) 11639–11645.
[47] M. Islam, D.S.K. Ting, A. Fartaj, Aerodynamic models for Darrieus-type straight-bladed vertical axis wind turbines, Renew. Sust. Energ. Rev. 12 (2008) 1087–1109.
[48] M. Xiao, L. Wang, F.Q. Ji, F. Shi, Converting chemical energy to electricity through a three-jaw mini-generator driven by the decomposition of hydrogen peroxide, ACS Appl. Mater. Interfaces 8 (2016) 11403–11411.
[49] S.K. Sailapu, A. Chattopadhyay, Induction of electromotive force by an autonomously moving magnetic bot, Angew. Chem. Int. Ed. 53 (2014) 1521–1524.
[50] J.E. Poelma, B.P. Fors, G.F. Meyers, J.W. Kramer, C.J. Hawker, Fabrication of complex three-dimensional polymer brush nanostructures through light-mediated living radical polymerization, Angew. Chem. Int. Ed. 52 (2013) 6844–6848.
[51] Y. Yang, H.L. Luo, J.L. Yang, D.F. Huang, S.X. Zhou, Facile UV-curing technique to establish a 3D-grafted poly(ethylene glycol) layer on an epoxy resin base for underwater applications, J. Appl. Polym. Sci. 133 (2016) 43972.

Biographies

Wei Guan is a Master from Jilin University, China. Her research interest lies in environment-induced microactuators based on femtosecond laser fabrication.

Chao Lv received her PhD degree in electronics from Jilin University. Her research interests include stimulus-responsive hydrogels and soft actuators.

Yi-Shi Xu is a Master from Jilin University, China. His research interests include organic crystal and nanofabrication.

Yan-Hao Yu received his PhD degree in electronics from Jilin University, China, in 2016. His research interest focuses on laser microfabrication.

Hong Xia received her PhD degree in Chemistry from Jilin University, China, in 2006. She is currently a full professor at Jilin University. Her research interests include intelligent materials, stimulus-responsive actuators and laser microfabrication.

Li-Gang Niu received his PhD degree in electronics from Jilin University, China. His research interest lies in 3D micronanofabrication by laser.

Sen Liu is a Master from Jilin University, China. His research interest lies in light-driven microactuators based on laser fabrication.

Gong Wang is currently a Master student at Jilin University, China. His research interests include the field of piezoelectric polymer, controlled deformations of soft actuators, energy device for energy conversion.

Ying-Shuai Wang received his PhD degree in electronics from Jilin University, China, in 2017. His research interests lie in the field of micro motor and application of nanocomposites.

Hong-Bo Sun received the B.S. and the Ph.D. degrees in electronics from Jilin University, China, in1992 and 1996, respectively. He worked as a postdoctoral researcher in Satellite Venture Business Laboratory, the University of Tokushima, Japan, from 1996 to 2000, and then as an assistant professor in Department of Applied Physics, Osaka University, Japan. In 2004, he was promoted as a full professor (Changjiang Scholar) in Jilin University, and since 2017 he has been working in Tsinghua University, China. His research interests have been focused on ultrafast optoelectronics, particularly on laser nanofabrication and ultrafast spectroscopy: Fabrication of various micro-optical, microelectronical, micromechanical, micro-optoelectronic, microfluidic components and their integrated systems at nanoscale, and exploring ultrafast dynamics of photons, electrons, phonons, and surface plasmons in solar cells, organic light-emitting devices and low-dimensional quantum systems at femtosecond timescale. So far, he has published over 350 scientific papers in the above fields, which have been cited for more than 12000 times according to ISI search report. He is currently the topical editor of Optics Letters (OSA), Light: Science and Applications (Nature Publishing Group), Chinese Science Bulletin (Springer), and editorial advisory board member of Nanoscale (RSC) and Display and Imaging (Old City Publishing).